Rapid generation of metastable helium Bose-Einstein condensates

A. H. Abbas,[1,2] X. Meng [ORCID],[1] R. S. Patil,[1,3,*] J. A. Ross [ORCID],[1] A. G. Truscott,[1] and S. S. Hodgman[1,†]

[1]*Research School of Physics, Australian National University, Canberra 0200, Australia*
[2]*Department of Physics, Faculty of Science, Cairo University, Giza, Egypt*
[3]*Indian Institute of Science Education and Research, Pune 411008, India*

We report the realization of Bose-Einstein condensation (BEC) of metastable helium atoms using an in-vacuum coil magnetic trap and a crossed-beam optical dipole trap. A quadrupole-Ioffe configuration magnetic trap made from in-vacuum hollow copper tubes provides fast switching times while generating traps with a 10-G bias, without compromising optical access. The bias enables in-trap one-dimensional Doppler cooling to be used, which is the only cooling stage between the magneto-optic trap and the optical dipole trap. This allows direct transfer to the dipole trap without the need for any additional evaporative cooling in the magnetic trap. The entire experimental sequence takes 3.3 s, with essentially pure BECs observed with $\sim 10^6$ atoms after evaporative cooling in the dipole trap.

The experimental creation of Bose-Einstein condensates (BECs) of dilute weakly interacting gases of atoms [1–3] has opened the possibility of exploring interesting phenomena of the quantum world on a macroscopic scale. Over subsequent years the field has exploded, with BECs now used in diverse fields of quantum science, including quantum many-body systems [4], topological physics [5], and precision inertial measurements [6]. While BEC experiments were initially limited to observing collective properties of the ensemble, a number of more recent detection techniques allow for the detection of individual atoms [7], opening up a broad range of experimental possibilities. In experiments involving alkali or rare-earth atoms, such single-atom detection is usually performed via high-resolution fluorescence imaging, either *in situ* in optical lattices [8,9] or after expansion from a trap [10,11]. However, such techniques usually have limitations on their spatial extent and the atom number able to be imaged.

An alternative method of single-atom detection exploits the high internal energy of helium atoms trapped in the first atomic excited 2^3S_1 metastable state (He*), which has 19.8 eV of internal energy. The high internal energy allows direct detection of individual atoms with full three-dimensional (3D) resolution using electronic detectors such as multichannel plate and delay-line detectors (MCP-DLD) [12]. This has opened up a wide range of exciting experimental possibilities, allowing quantum-optics equivalent demonstrations with atoms of iconic experiments such as the Hanbury Brown-Twiss (HBT) effect [13], Wheeler's delayed choice [14], the Hong-Ou-Mandel effect [15], ghost imaging [16], and the measurement of Bell correlations [17]. More than just replicating quantum optics, though, the atomic interactions allow

effects to be seen that are not possible with photons, such as fermionic antibunching [18], quantum depletion [19], and strongly interacting lattice physics [20].

Crucial to many of these experiments are the measurements of HBT-style correlation functions—the key observable enabled by single-atom detection. However, such correlation functions require large amounts of data, especially if higher-order correlations are being measured [21,22], often needing 10,000–100,000 individual experimental runs for a single experiment. This has led to constant improvements across generations of experimental He* apparatuses aiming for ever-shorter experimental sequences. Most He* experiments [23–27] use magnetic traps, where the sequence length is limited by the slow thermalization rates in magnetic traps that have relatively weak trap frequencies. While using liquid helium in the source stage can substantially reduce the sequence length [26], it is less practical for everyday operation. The tight traps provided by dipole traps can overcome this, either in a hybrid combination with a magnetic trap [28] or in a stand-alone cross-beam configuration [29]. However, due to the limited depth of the dipole trap, to enable an efficient transfer the atoms need to first be cooled, either optically via complex additional cooling schemes such as gray molasses and/or evaporatively in a magnetic trap [29].

In this work we report on the construction of a He* BEC machine capable of creating condensates in a simplified, rapid sequence that takes only 3.3 s in total. An initial stage of one-dimensional (1D) Doppler cooling [25] is performed in a biased magnetic trap, constructed using a simplified in-vacuum water-cooled coil geometry to produce a biased quadrupole trap. This lowers the temperature enough to permit direct loading of a crossed dipole trap, which allows fast and efficient evaporative cooling. The final BECs are produced with 10^6 atoms. Our method gives us around a factor of 2 improvement in both BEC atom number and sequence duration compared to that reported for a similar experimental

---
[*]Present address: Department of Physics, The Pennsylvania State University, University Park, Pennsylvania 16802, USA.
[†]sean.hodgman@anu.edu.au
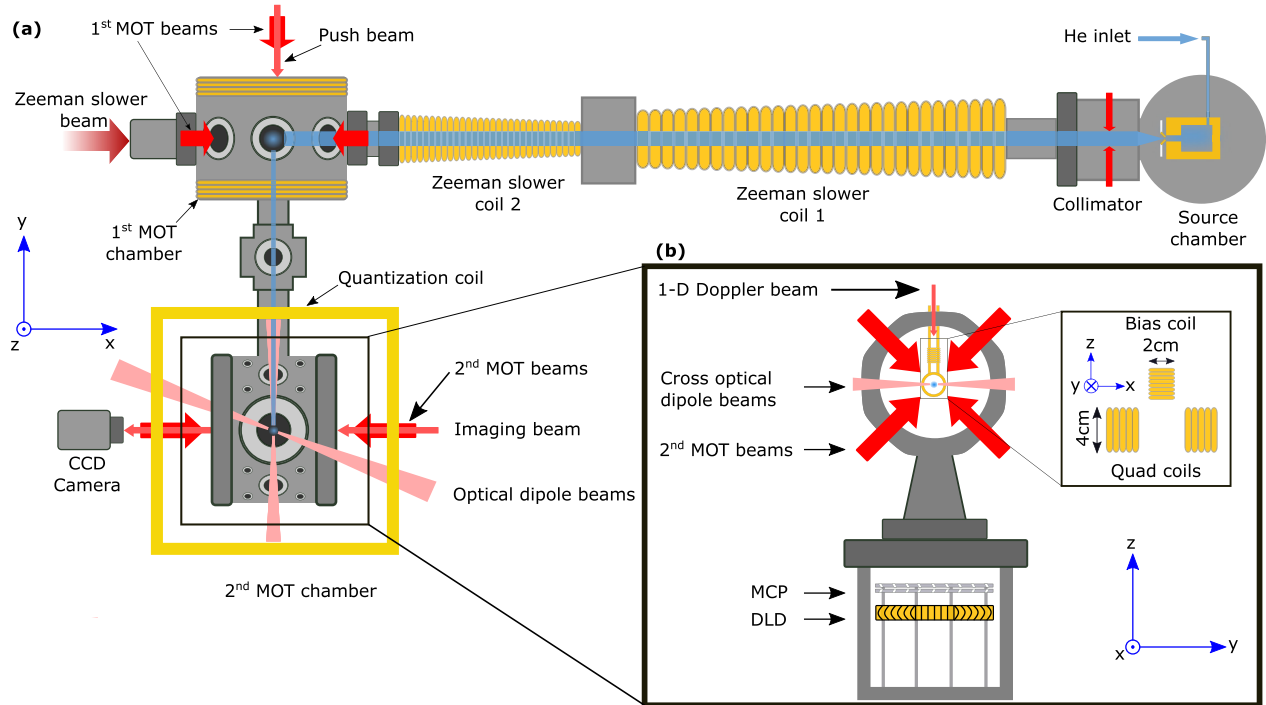
FIG. 1. Schematic of the experimental apparatus (see main text for details). (a) Top view of the experimental setup. A beam of He* atoms is produced in a cryogenically liquid-nitrogen-cooled source, before being optically collimated, slowed, and cooled in a first MOT stage. This forms a source for the second MOT, where the atoms are then transferred to a magnetic trap and subsequently to an optical dipole trap, where the BEC is generated. (b) Side view of the second MOT chamber, showing the quadruple-Ioffe configuration in-vacuum trap and MCP-DLD detector. The inset shows the trapping coil geometry from a different angle.

setup [29], while avoiding the complication of a gray molasses stage required in that experiment. In addition to the relatively small size and minimal number of coil turns, which allow fast switch-off times, a major advantage of this magnetic trap design is that the small size allows good optical access to the atomic cloud and thus a large numerical aperture of NA ∼0.4. This will make the apparatus ideal for future optical lattice experiments [20].

A number of magnetic trap designs are used in BEC experiments, with some commonly used ones including the cloverleaf design [30], the quadrupole-Ioffe configuration (QUIC) trap [31], and atomic chip traps [32]. Any design has strengths and weaknesses, and inevitably involves compromises and tradeoffs between factors such as confinement, depth, stability, switch-off time, physical size, current required, and heat dissipation. In our magnetic trap setup, no evaporation is implemented; we only perform 1D Doppler cooling in the trap. Hence we require a large enough bias to split the atomic energy levels (as well as prevent Majorana and Penning losses) but are not so concerned about the usual consideration of having a tight confinement, as all evaporation is conducted in the dipole trap. The trap is in a simple QUIC configuration, consisting of two 5-turn anti-Helmholtz (AH) coils of 40-mm diameter centered on the y axis and an 8-turn bias coil of 20-mm diameter centered on the z axis, as shown in Fig. 1. These coils are made from 2-mm hollow copper tubing (internal diameter 0.4 mm) mounted in-vacuum to ensure they are close to the atoms. While other experiments have used in-vacuum mounted atom chip traps [32] and Ioffe-Pritchard configuration traps [33], this is an in-vacuum realization of

a QUIC trap. Cooling is provided by pumping chilled water through the tubes, with each tube attached to hollowed out 1/4-inch feedthroughs sealed with vacuum-compatible solder [34]. By driving 120 A through the AH coils and 62 A though the bias we were able to produce a trap of ∼1.6 mK depth and 10-G bias field (see Fig. 2) in the trap center, which is offset 6 mm vertically along the z axis from the center
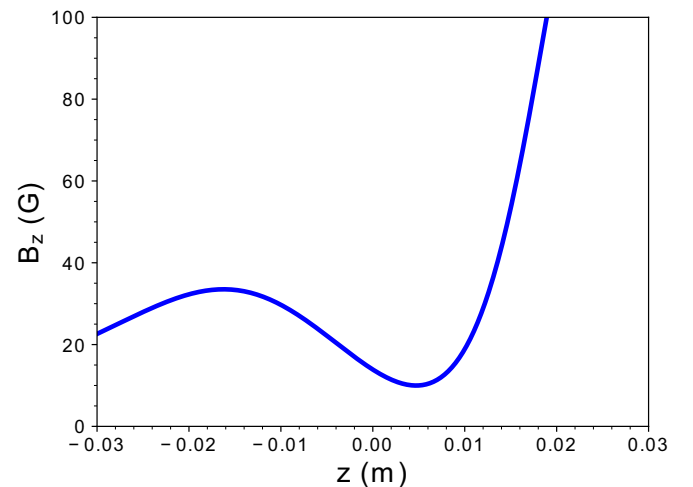

FIG. 2. The magnetic trap potential along the vertical axis $\hat{z}$ for our in-vacuum magnetic trap. The trap minimum is 10 Gauss located 6 mm above the center of the quadrupole coils, while the total trap depth is ∼25 Gauss, equivalent to 1.6 mK.
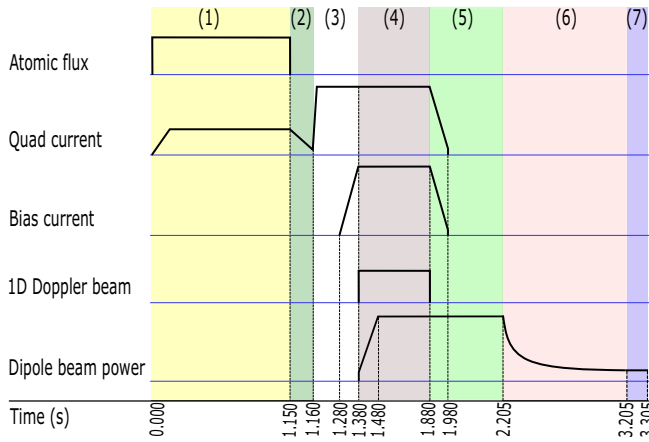
FIG. 3. The timings of important stages of the experimental BEC production sequence. (1) the MOT is first loaded from the atomic flux (in the diagram representing Zeeman slower, first MOT etc.). The MOT is then compressed (2) prior to loading into the biased magnetic trap (3). 1D Doppler cooling is then performed in the magnetic trap (4), which is subsequently ramped down for transfer to the dipole trap (5). Finally, an evaporative cooling stage (6) in the dipole trap is followed by a short hold (7) to ensure the atoms are thermalized before the dipole trap is switched off and the atoms fall onto the MCP-DLD detector. Note that to help with visualization, the time axis is not to scale.

of the AH coils. The radial and axial trap frequencies are $\omega_\perp = 2\pi \times 89$ Hz in the radial axes and $\omega_z = 2\pi \times 57$ Hz, respectively.

The timing of the experimental sequence is shown in Fig. 3. A cold source of He* atoms suitable for loading into a magneto-optic trap (MOT) is generated from our He* beamline, shown schematically in Fig. 1. Helium atoms are excited into the metastable state via a hollow cathode DC discharge source [35] which is cryogenically cooled using liquid nitrogen. The expanding atomic beam is then collimated using an optical collimation stage featuring four beams propagating perpendicular to the He* atoms with an intensity $\sim 67 I_{sat}$ ($I_{sat} = 0.167$ mW/cm^2) and detuned by $\sim -5\Gamma$ ($\Gamma/2\pi = 1.63$ MHz) from resonance. Note that all detunings for laser cooling and imaging in this work are relative to the $2^3 S_1 \rightarrow 2^3 P_2$ transition at a wavelength of 1083.33 nm, with a negative sign indicating red detuning. All laser cooling and imaging beams are sourced from a home-built external gain-chip laser [36] with linewidth <100 kHz, which is used to seed a 5-W fiber amplifier. Individual frequency shifts are provided by acousto-optic modulators in each cooling beam. A Zeeman slower consisting of two separate coils is then employed to reduce the velocity of the atoms to <100 m/s, featuring a beam of $\sim 92 I_{sat}$ intensity and $\sim -160\Gamma$ detuning, counterpropagating with the direction of the atomic beam. A spatially varying field to keep the atoms on resonance while they slow down is generated by two separate coils with variable windings along their length and a zero field in the center. These atoms are then trapped and cooled by the first MOT, with the three counterpropagating MOT beams having $\sim 87 I_{sat}$ intensity (horizontal beam), 140 and 110I_{sat} intensity (vertical beams), all with $\sim -22\Gamma$ detuning.

However, the background pressure from the source is too high for this chamber to be used to form a BEC. The horizontal MOT retro mirror located inside the vacuum chamber has a ~ 1.5-mm-diameter hole in the center, which enables atoms to leak out of the MOT and into the UHV second MOT chamber, where the pressure is $<5 \times 10^{-11}$ Torr. To assist this process, an additional "push" beam is added ($\sim 110 I_{sat}$ intensity and $\sim 3.3\Gamma$ blue detuned), forming a low-velocity intense source scheme (LVIS) with a velocity of ~ 40 m/s [26]. The atomic flux from the LVIS, as measured ~ 10 cm beyond the location of the second MOT using a Faraday cup on a rotation stage and a picoammeter, is $\sim 9 \times 10^8$ atoms/s.

The second MOT consists of a quadrupole magnetic field generated by our in-vacuum AH coils with a gradient along the tight axis of $B' \sim 4.4$ G/cm, along with three pairs of counterpropagating laser beams with detunings $\Delta \sim -33\Gamma$ and intensities of $\sim 140 I_{sat}$, $\sim 37 I_{sat}$, and $\sim 400 I_{sat}$. In 1.15 s we load a cloud with $\sim 1.7 \times 10^8$ atoms at a temperature of ~ 2.5 mK. The atom number is measured using saturated fluorescence on an InGaAs photodiode [26]. To measure the temperature, we switch off the MOT and allow the atoms to fall ~ 451 mm onto a detector comprising an 80-mm-diameter stacked pair of multichannel plates. By using pick-off electronics, we extract a signal pulse from the charge depletion of the plates that each atom causes. After fast amplification and discrimination of the pulses, they are recorded using a digital counter, which provides an integrated 1D time-of-flight (TOF) distribution of the atoms. The TOF distribution is fitted to a Maxwell-Boltzmann distribution, given by [26,37]

$$n(t) = A v_0^2 \pi \left(\frac{(gt^2/2 + l_0)}{t^2} \right) \exp \left(-\frac{(gt^2/2 - l_0)^2}{v_0^2 t^2} \right), \quad (1)$$

where $A = (m/2\pi kT)^{3/2}$, $v_0 = \sqrt{(2kT/m)}$, m is the mass of a ^{4}He atom, k is Boltzmann's constant, and l_0 is the falling distance. From this distribution we extract the temperature T, with the only other free fit parameter being the amplitude A.

Following loading, the MOT is then compressed by ramping the magnetic field down to 1.4 G/cm in 10 ms, while simultaneously the laser detuning is ramped up to $\Delta \sim -0.4\Gamma$ and the intensity of the MOT beams are reduced by 2 orders of magnitude. The MOT beams are then switched off and the atoms in the $m_J = +1$ state remain trapped in the quadrupole magnetic field of the AH coils. To improve the trap depth and atom density, we tighten the quadrupole field to 16.6 G/cm in 100 μs. The bias coil current is then ramped up in 100 ms to form a QUIC trap with a 10-G field offset, removing the magnetic field zero in the quadrupole trap. This configuration provides weak trapping frequencies of $\omega_r \sim 2\pi \times 89$ Hz in the radial (x-y) direction and $\omega_z \sim 2\pi \times 57$ Hz in the axial (z) direction. At this stage we have $\sim 5.3 \times 10^7$ atoms at ~ 0.44 mK, with the lower temperature mostly due to the reduced magnetic trap depth compared to the MOT. The atom number and temperature in the magnetic trap are measured via absorption imaging, with the imaging beam along the x axis being imaged on an InGaAs CCD camera. Mechanical flipper mirrors allow us to swap between imaging and MOT beams on the same axis, although this prevents absorption imaging during the operation of the MOT.
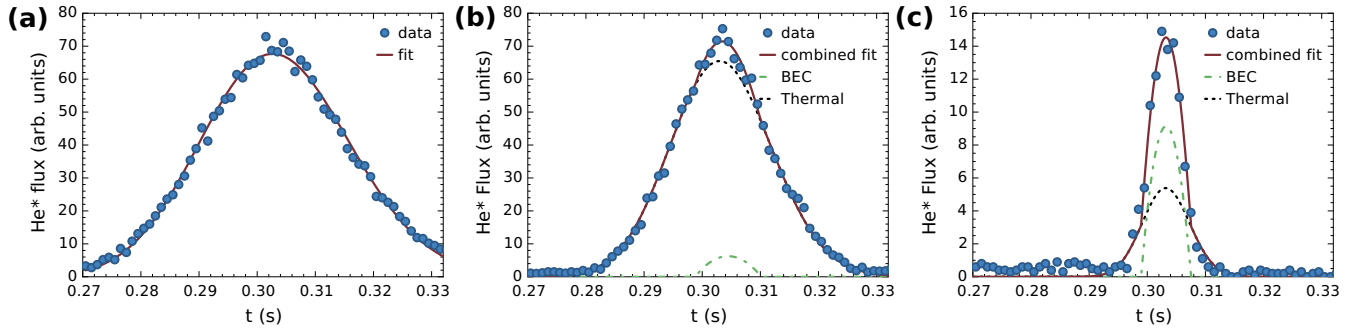
FIG. 4. Time-of-flight signal traces taken from the MCP after the dipole trap is switched off and atoms are allowed to fall onto the detector. The three plots show different points in the evaporation sequence. Data is shown as blue circles, with fits shown in red. Above T_c the fit is to a Maxwell-Boltzmann distribution (see text for details), while below T_c a parabolic Thomas-Fermi fit to the BEC component (green dot-dash line) is added to the thermal fit (black dashed line). The conditions for the plots shown: (a) reduced temperature $T/T_c = 1.02(5)$, trap frequencies $\omega_{x,y,z} \sim 2\pi \times (1100, 920, 1400)$ Hz, total atom number $N = 3.3(2) \times 10^6$. (b) $T/T_c = 0.88(7)$, $\omega_{x,y,z} \sim 2\pi \times (720, 590, 940)$ Hz, $N = 1.7(2) \times 10^6$, condensate atom number $N_0 = 0.2(1) \times 10^6$. (c) $T/T_c = 0.54(6)$, $\omega_{x,y,z} \sim 2\pi \times (320, 160, 360)$ Hz, $N = 1.5(5) \times 10^6$, $N_0 = 1.2(4) \times 10^6$. Each image represents data from 20 shots.

To cool the cloud further it is illuminated with a 1D Doppler cooling beam [25] of intensity $\sim 0.01 I_{\text{sat}}$, aligned vertically along the bias field axis, circularly polarized to drive the σ^+ transition and red detuned by $\sim -\Gamma/2$. This Doppler cooling stage cools the cloud in 500 ms, after which we have $\sim 4.9 \times 10^7$ atoms at $\sim 83\,\mu$K, approaching the Doppler limit for He* of 39 μK [12]. This is sufficiently cold to directly transfer the atoms from the magnetic trap to the crossed optical dipole trap.

The final trapping stage is a crossed optical dipole trap (CODT), formed from two intersecting laser beams. These beams are far detuned from the 1083-nm helium resonance at 1550-nm wavelength and originate from a 100-kHz linewidth seed laser that is amplified to 30 W of total power. The power is distributed between the two beams such that after feedback loops to regulate the intensity and losses due to acousto-optic modulator and fiber coupling, the first beam (aligned along the y axis) has up to 6 W and the second beam (aligned $\sim 10°$ from the x axis in the x-y plane) has up to 1 W of power. These beams are focused down to Gaussian $1/e^2$ waists of 73 and 55 μm, respectively, at the location of the atoms. The two beams intersect at the center of the 10-G biased QUIC trap, forming a CODT with trapping frequencies $\omega_{x,y,z} \sim 2\pi \times (1.1, 1.2, 1.7)$ kHz and a trap depth of $\sim 150\,\mu$K at full power.

Since the 1D Doppler cooling process is more efficient at higher densities [25], we observe that the Doppler cooling is more effective with the dipole beams on, in addition to the magnetic trap. Here the dipole beams mostly serve to increase the density of the atomic cloud, making the cooling process more efficient and reducing the final temperature after 1D Doppler cooling. In our experiment, this improves the final atom number by $\sim 50\%$. Hence the dipole beams are linearly increased to full power over 100 ms prior to the start of the 1D Doppler cooling stage. To transfer the atoms from the QUIC to the dipole trap, after the 1D Doppler cooling stage the trap is linearly decreased in 100 ms to a nonbiased trap with ~ 1.1 G/cm gradient along the tight axis, before being abruptly turned off with a field-effect-transistor switch. To preserve the quantization axis of the atoms and prevent any

spin flips during this switch off, an additional large (~ 50 cm diameter square) coil mounted above the vacuum chamber was used to generate a uniform magnetic field of ~ 1.6 G aligned along the $\hat{z}$ direction. This field is switched on before the current through the QUIC trap starts ramping down. However, once in the dipole trap, it was found that the background magnetic field (dominated by the z component of the Earth's magnetic field) was sufficient to preserve the quantization, so the extra quantization coil was switched off 700 ms after transfer to the CODT. Immediately after transfer we measure $\sim 5 \times 10^6$ atoms at $13.5(1)\mu$K with a phase-space density of ~ 0.5 in the CODT, an excellent starting point for runaway evaporative cooling.

Evaporation is performed in the CODT by lowering the trap depth through reducing the power of the dipole beams exponentially over 1 s. As the hotter atoms escape and the remaining atoms rethermalize, this reduces the temperature and enhances the phase-space density. The evaporation duration is set by the relatively high trap frequencies (and thus high rethermalization rates). Unlike in a previous similar He* experiment [29], we did not observe any improvement in the evaporation process by adding a gradient to cancel the weak components of the dipole potentials along the beam propagation directions.

To determine the important parameters of the gas in the CODT, we switch off the dipole trap and allow the atoms to fall under gravity onto the MCP to measure the 1D TOF profile along the z axis, integrated in the x-y dimensions. Examples of the resulting integrated 1D TOF profiles are shown in Fig. 4. Above the condensation critical temperature T_c^* (note that T_c refers to the noninteracting critical temperature, while T_c^* is the critical temperature corrected for interactions [38]), the profile is fitted to the same Maxwell-Boltzmann distribution as in Eq. (1) to yield the temperature T. Below T_c^* we fit with a bimodal distribution consisting of the same Maxwell-Boltzmann distribution plus an inverted parabola to represent the far-field Thomas-Fermi density profile of the BEC [38]. The half width of this parabola is the far-field Thomas-Fermi radius R_{TF}, from which we can extract the chemical potential μ from $\mu \approx m R_{TF}^2 / 2 t_{TOF}^2$ [39]. From the
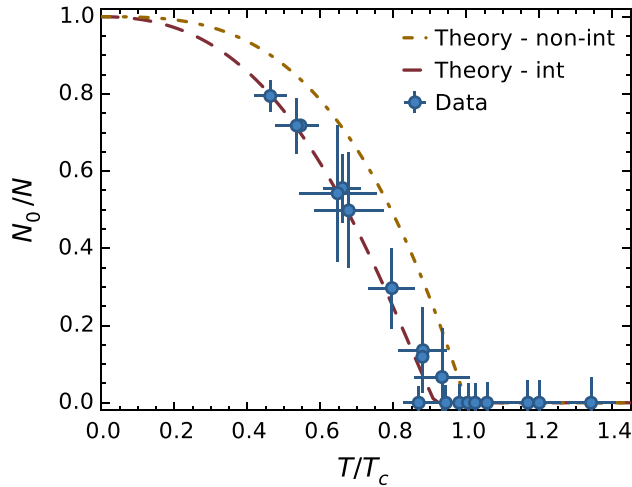
FIG. 5. Condensate fraction N_0/N vs reduced temperature T/T_c for different points in the evaporation sequence. Data are shown as blue points, with error bars dominated by fit uncertainties due to the condensate and thermal widths being relatively similar for many data points, making accurate fits difficult. The brown dot-dash line shows the noninteracting theory, while the red dashed line shows a correction accounting for two-body interactions [38]. For $N_0/N \gtrsim 0.8$ the thermal component is obscured by the condensate, which prevents reliable fits, hence the final evaporation points are not shown.

chemical potential we can extract the number of atoms in the condensate $N_0 = (2\mu)^{5/2}/15\sqrt{m}\hbar^2\bar{\omega}^3 a$, where a is the He*s-wave scattering length. The number of atoms in the thermal cloud N_T is given by $N_T \approx 1.202(k_B T/\hbar\bar{\omega})^3$ for $T < T_c^*$. To extract the atom number above T_c^*, we sum the integrated counts, correct for the fraction of the cloud at temperature T that will hit the detector, and then scale by an effective quantum efficiency of the detector γ_{QE}. We vary γ_{QE} until the thermal atom number N_T matches for the clouds

just above and below T_c^*. Note that nonlinearities in γ_{QE} at high fluxes mean this would not be an accurate method to determine N_0.

The above information, along with the total atom number $N = N_0 + N_T$ and $k_B T_c = 0.94\hbar\bar{\omega}N^{1/3}$, is then combined to produce Fig. 5. This shows the condensate fraction N_0/N vs the reduced temperature T/T_c for our sequence as we evaporate through the transition temperature. We cross T_c^* at $\sim 6~\mu K$ with $\sim 3 \times 10^6$ atoms, and by evaporating further we are able to produce BECs with no discernible thermal fraction (not shown on the graph) with $\sim 1 \times 10^6$ atoms.

We demonstrate a comparatively simple and short method for producing Bose-Einstein condensates of He* atoms. By using a magnetic trap with a 10-G bias generated from an in-vacuum set of coils, we are able to cool the cloud below $100~\mu K$ in the magnetic trap via 1D Doppler cooling. The degenerate state of metastable helium atoms is accomplished via direct evaporative cooling in a crossed optical dipole trap. We cross the condensation critical temperature with $\sim 3 \times 10^6$ atoms at $\sim 6~\mu K$ and by evaporating further are able to generate essentially pure BECs with $\sim 1 \times 10^6$ atoms. The entire sequence to produce a BEC only takes 3.3 s, allowing us to produce BECs with twice as many atoms in nearly half the time of [29], with our setup also being technically less complex. This will provide an excellent starting point for a range of experiments with He* BECs, such as many-body correlation experiments [22], probes of quantum nonlocality [17], or strongly interacting optical lattice physics [20].

[1] M. H. Anderson, J. R. Ensher, M. R. Matthews, C. E. Wieman, and E. A. Cornell, Science **269**, 198 (1995).

[2] C. C. Bradley, C. A. Sackett, J. J. Tollett, and R. G. Hulet, Phys. Rev. Lett. **75**, 1687 (1995).

[3] K. B. Davis, M. O. Mewes, M. R. Andrews, N. J. van Druten, D. S. Durfee, D. M. Kurn, and W. Ketterle, Phys. Rev. Lett. **75**, 3969 (1995).

[4] I. Bloch, J. Dalibard, and W. Zwerger, Rev. Mod. Phys. **80**, 885 (2008).

[5] N. R. Cooper, J. Dalibard, and I. B. Spielman, Rev. Mod. Phys. **91**, 015005 (2019).

[6] R. Geiger, A. Landragin, S. Merlet, and F. Pereira Dos Santos, AVS Quantum Sci. **2**, 024702 (2020).

[7] H. Ott, Rep. Prog. Phys. **79**, 054401 (2016).

[8] W. S. Bakr, J. I. Gillen, A. Peng, S. Fölling, and M. Greiner, Nature (London) **462**, 74 (2009).

[9] J. F. Sherson, C. Weitenberg, M. Endres, M. Cheneau, I. Bloch, and S. Kuhr, Nature (London) **467**, 68 (2010).

[10] R. Bücker, A. Perrin, S. Manz, T. Betz, C. Koller, T. Plisson, J. Rottmann, T. Schumm, and J. Schmiedmayer, New J. Phys. **11**, 103039 (2009).

[11] A. Bergschneider, V. M. Klinkhamer, J. H. Becher, R. Klemt, G. Zürn, P. M. Preiss, and S. Jochim, Phys. Rev. A **97**, 063613 (2018).

[12] W. Vassen, C. Cohen-Tannoudji, M. Leduc, D. Boiron, C. I. Westbrook, A. Truscott, K. Baldwin, G. Birkl, P. Cancio, and M. Trippenbach, Rev. Mod. Phys. **84**, 175 (2012).

[13] M. Schellekens, R. Hoppeler, A. Perrin, J. V. Gomes, D. Boiron, A. Aspect, and C. I. Westbrook, Science **310**, 648 (2005).

[14] A. G. Manning, R. I. Khakimov, R. G. Dall, and A. G. Truscott, Nat. Phys. **11**, 539 (2015).

[15] R. Lopes, A. Imanaliev, A. Aspect, M. Cheneau, D. Boiron, and C. I. Westbrook, Nature (London) **520**, 66 (2015).

[16] R. I. Khakimov, B. M. Henson, D. K. Shin, S. S. Hodgman, R. G. Dall, K. G. H. Baldwin, and A. G. Truscott, Nature (London) **540**, 100 (2016).

[17] D. K. Shin, B. M. Henson, S. S. Hodgman, T. Wasak, J. Chwedenczuk, and A. G. Truscott, Nat. Commun. **10**, 4447 (2019).

[18] T. Jeltes, J. M. McNamara, W. Hogervorst, W. Vassen, V. Krachmalnicoff, M. Schellekens, A. Perrin, H. Chang, D. Boiron, A. Aspect, and C. I. Westbrook, Nature (London) **445**, 402 (2007).

[19] R. Chang, Q. Bouton, H. Cayla, C. Qu, A. Aspect, C. I. Westbrook, and D. Clément, Phys. Rev. Lett. **117**, 235303 (2016).

[20] H. Cayla, S. Butera, C. Carcy, A. Tenart, G. Hercé, M. Mancini, A. Aspect, I. Carusotto, and D. Clément, Phys. Rev. Lett. **125**, 165301 (2020).

[21] R. G. Dall, A. G. Manning, S. S. Hodgman, Wu RuGway, K. V. Kheruntsyan, and A. G. Truscott, Nat. Phys. **9**, 341 (2013).

[22] S. S. Hodgman, R. I. Khakimov, R. J. Lewis-Swan, A. G. Truscott, and K. V. Kheruntsyan, Phys. Rev. Lett. **118**, 240402 (2017).

[23] A. Robert, O. Sirjean, A. Browaeys, J. Poupard, S. Nowak, D. Boiron, C. I. Westbrook, and A. Aspect, Science **292**, 461 (2001).

[24] F. Pereira Dos Santos, J. Léonard, J. Wang, C. J. Barrelet, F. Perales, E. Rasel, C. S. Unnikrishnan, M. Leduc, and C. Cohen-Tannoudji, Phys. Rev. Lett. **86**, 3459 (2001).

[25] A. S. Tychkov, T. Jeltes, J. M. McNamara, P. J. J. Tol, N. Herschbach, W. Hogervorst, and W. Vassen, Phys. Rev. A **73**, 031603(R) (2006).

[26] R. Dall and A. Truscott, Opt. Commun. **270**, 255 (2007).

[27] M. Keller, M. Kotyrba, F. Leupold, M. Singh, M. Ebner, and A. Zeilinger, Phys. Rev. A **90**, 063607 (2014).

[28] A. S. Flores, H. P. Mishra, W. Vassen, and S. Knoop, Appl. Phys. B **121**, 391 (2015).

[29] Q. Bouton, R. Chang, A. L. Hoendervanger, F. Nogrette, A. Aspect, C. I. Westbrook, and D. Clément, Phys. Rev. A **91**, 061402(R) (2015).

[30] M.-O. Mewes, M. R. Andrews, N. J. van Druten, D. M. Kurn, D. S. Durfee, and W. Ketterle, Phys. Rev. Lett. **77**, 416 (1996).

[31] T. Esslinger, I. Bloch, and T. W. Hänsch, Phys. Rev. A **58**, R2664 (1998).

[32] J. Fortágh and C. Zimmermann, Rev. Mod. Phys. **79**, 235 (2007).

[33] K. Moore, T. Purdy, K. Murch, K. Brown, K. Dani, S. Gupta, and D. Stamper-Kurn, Appl. Phys. B **82**, 533 (2006).

[34] Note that standard solder and flux was also found to work, although requiring an initial period under vacuum to remove the residual flux before being installed in the final UHV chamber. This reduced outgassing from the non-vacuum-compatible flux to a level sufficient to reach UHV pressures.

[35] J. Swansson, K. Baldwin, M. Hoogerland, A. Truscott, and S. Buckman, Appl. Phys. B **79**, 485 (2004).

[36] D. K. Shin, B. M. Henson, R. I. Khakimov, J. A. Ross, C. J. Dedman, S. S. Hodgman, K. G. H. Baldwin, and A. G. Truscott, Opt. Express **24**, 27403 (2016).

[37] I. Yavin, M. Weel, A. Andreyuk, and A. Kumarakrishnan, Am. J. Phys. **70**, 149 (2002).

[38] F. Dalfovo, S. Giorgini, L. P. Pitaevskii, and S. Stringari, Rev. Mod. Phys. **71**, 463 (1999).

[39] While this approximation for the chemical potential from the far-field R_{TF} is only valid for condensates in cigar-shaped traps, numerical solutions of the equations of motion following [40] show that it gives at most an $\approx 10\%$ error in μ for the trap geometries in our system, which is within our experimental uncertainties.

[40] Y. Castin and R. Dum, Phys. Rev. Lett. **77**, 5315 (1996).